



Design Procedure for a Broadband TE_{11}/HE_{11} Mode Converter for High-Power Radar Applications

Daniel Haas¹  · Manfred Thumm^{1,2}

Received: 21 November 2020 / Accepted: 11 January 2021 / Published online: 09 March 2021
© The Author(s) 2021

Abstract

The HE_{11} hybrid mode, propagating in an overmoded corrugated circular waveguide, is widely used for low loss transmission of high-power microwaves. Due to the inherent broadband frequency behaviour, this will be also essential for future broadband high-power radar applications, like space debris observation in low earth orbit (LEO). A promising amplifier concept for such radar sensors is a helical gyro-TWT. However, since the HE_{11} hybrid mode is not suitable for electron-beam-wave interaction in this kind of vacuum electron device, an additional mode converter is required. The present paper addresses the design procedure of a broadband high-power mode converter, designed for a helical gyro-TWT intended for future broadband high-power radar applications in the W-band. The interaction mode of the helical gyro-TWT under consideration can be easily transferred to the circular waveguide TE_{11} mode. Therefore, a $TE_{11} \leftrightarrow HE_{11}$ mode converter is addressed here. The design procedure is based on a scattering matrix formalism and leads to a high HE_{11} mode content of $\geq 98.6\%$ within the considered frequency range from 92 GHz to 100 GHz. Inside this frequency band, the mode content is even better and reaches $\approx 99.7\%$ at ≈ 95 GHz. This allows broadband frequency operation of a helical gyro-TWT and is suitable for broadband high-power radar applications.

Keywords Mode converter · Hybrid modes · Helical Gyro-TWT · W-Band · Radar · Space debris

1 Introduction

Helical gyro-TWTs are considered as promising broadband high-power amplifiers for future microwave applications, like advanced radar sensors for space debris observation in low earth orbit (LEO). Due to the enormous progress in the field of high-power microwave

✉ Daniel Haas
daniel.haas@kit.edu

¹ IHM, Karlsruhe Institute of Technology (KIT), Kaiserstr. 12, D-76131 Karlsruhe, Germany

² IHE, Karlsruhe Institute of Technology (KIT), Kaiserstr. 12, D-76131 Karlsruhe, Germany

technology [1, 2], corresponding radar sensors can also be operated in high frequency bands such as the W-band [3, 4]. Due to the high bandwidth available there, very high resolutions can be achieved [3–5]. In near future, even W-band transmission powers in the range of 10 kW to 100 kW may be possible [6]. To realize a W-band radar sensor with such a high transmission power, a suitable high-power amplifier as well as an appropriate transmission line is required. The transmission line connects the output of the high-power amplifier with the antenna feed. Due to the high power, oversized transmission lines are required. A suitable transmission mode is the HE_{11} hybrid mode, propagating in a corrugated circular waveguide. Low ohmic loss, small mode conversion, high degree of polarization and low-sidelobe radiation patterns can be achieved [7–9]. For transmission, the amplified microwave signal has to be converted into the HE_{11} hybrid mode, after leaving them interaction circuit. In a simple way, this may be realized due to a corrugated horn antenna [10, 11], illuminating the aperture of a highly overmoded circular waveguide [12, 13]. However, since the broadband frequency behaviour of the transmission line components may be sensitive in respect to the mode content [14, 15], a mode purity as best as possible is required, within the considered frequency range. A concept based on a corrugated horn antenna is limited in respect of the mode purity [12, 13]. Therefore, a waveguide mode converter is preferred here, which may attain a significant better mode purity [12]. The interaction mode for the helical gyro-TWT under consideration can be easily transferred to the circular waveguide TE_{11} mode [16]. Therefore, a $TE_{11} \rightarrow HE_{11}$ mode converter is addressed here. The frequency range from 92 GHz to 100 GHz is considered.

A corresponding mode converter may be realized employing a customized corrugation profile with varying groove depth within a corrugated waveguide [17, 18]. However, due to the small wavelength in the W-band and the required tiny geometry [17, 18], the technical realization of this type of mode transducer may be challenging. Therefore, a smooth-wall mode converter with customized diameter contour is discussed here. Its technical realization will be much simpler.

A similar mode converter, also for a high-power amplifier tube, was considered in [19]. However, there, a horn antenna concept to couple into the TEM_{00} free-space mode and another approach for optimization was chosen. To the best knowledge of the authors, a similar design procedure as addressed in the present paper has not yet been published elsewhere.

The paper is organized as follows: In Section 2 fundamental aspects are introduced, important for the following sections. Section 3 discusses the proposed design procedure and corresponding simulation results. Section 4 closes with a conclusion and an outlook for future research activities.

2 Fundamentals

To clarify the context of the present paper, Subsection 2.1 shortly discusses fundamental aspects of a helical gyro-TWT. The purpose of use and the location of the addressed mode converter within such a vacuum electron device is emphasized. A comprehensive introduction of helical gyro-TWTs can be found in [20–27]. In Subsection 2.2 calculations on hybrid modes in corrugated circular waveguides are addressed. In Subsection 2.3 equations for the decomposition of an arbitrary electromagnetic wave into the eigenmodes of a corrugated waveguide are given.

2.1 Helical Gyro-TWT

Amplification within a gyro-TWT is based on the electron cyclotron instability [24, 25]. Within the Brillouin diagram [28], those simplified resonance condition represents a straight line [24]. Electron-wave interaction occurs at points of intersection with the interaction mode [21–24]. A tangential intersection leads to broadband frequency operation [16, 21–24].

In a helical gyro-TWT, a customized helical interaction waveguide is used to generate an interaction mode which is tangential at close to zero axial wavenumber [1, 2, 20–23] with a close to constant group velocity [21] within the frequency band of interest. This leads to reduced sensitivity in respect of axial electron velocity spread, broadband frequency behaviour and improved stability [20–23]. For electron-wave interaction within a three-fold helical waveguide, typically a circularly polarized “quasi” TE₂₁ mode [6] is used. Its transversal field components are similar to the TE₂₁ mode within a circular waveguide, but the dispersion is tailored for broadband electron wave synchronization. After the electron-beam-wave interaction, the “quasi” TE₂₁ mode can be easily transferred to the fundamental circular waveguide TE₁₁ mode [16]. However, for low-loss transmission through to the vacuum window, the HE₁₁ mode is more suitable than the TE₁₁ mode. Therefore, an additional broadband high-power TE₁₁ → HE₁₁ mode converter is required.

As already mentioned, a smooth-wall mode converter with customized diameter contour is addressed here. Besides a simpler technical realization, this also allows to integrate an electron collector within the mode converter. This further simplifies the tube design. However, the corresponding collector design is out of scope of the present paper and will be addressed in more details in an upcoming paper.

At the mode converter output, a corrugated circular waveguide, able to propagate the HE₁₁ hybrid mode under the balanced hybrid mode condition [10], is flanged. No critical reflection or mode conversion has to be expected thereby. The vacuum window will be integrated within the corrugated waveguide.

2.2 Hybrid Modes in Corrugated Circular Waveguides

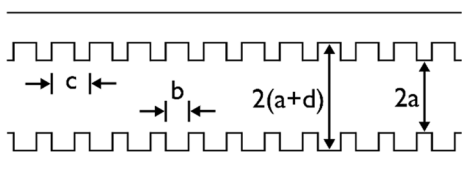
Figure 1 shows a simplified sketch of a corrugated circular waveguide with the radius *a*, the corrugation period *c*, the slot width *b* and the corrugation depth *d*.

The electromagnetic field components for *r* ≤ *a* may be written as:

$$\begin{aligned} \vec{E} &= \vec{E}^{\text{TE}} + \psi \cdot \vec{E}^{\text{TM}} \\ \vec{H} &= \vec{H}^{\text{TE}} + \psi \cdot \vec{H}^{\text{TM}} \end{aligned} \tag{1}$$

with:

Fig. 1 Corrugated waveguide with the waveguide radius *a*, the corrugation period *c*, the slot width *b* and the corrugation depth *d*



$$\begin{aligned}
 H_z^{\text{TE}} &= A^{\text{TE}} \cdot J_m\left(\frac{X}{a} \cdot r\right) \cdot \exp[-j\omega t] \cdot \left(\frac{\sin(m\varphi)}{\cos(m\varphi)}\right) \\
 E_z^{\text{TM}} &= A^{\text{TM}} \cdot J_m\left(\frac{X}{a} \cdot r\right) \cdot \exp[-j\omega t] \cdot \left(\frac{\cos(m\varphi)}{\sin(m\varphi)}\right)
 \end{aligned}
 \tag{2}$$

and $\psi = A^{\text{TM}}/A^{\text{TE}}$. The function $J_m(x)$ is the Bessel function of the first kind and the order m . The function $J'_m(x)$ is its first derivation in respect of x . Using the Maxwell equations [28], all remaining field components in Eq. (1) can be calculated based on Eq. (2) [28]. To avoid Bragg reflection, the angular field component at $r = a$ has to vanish [10, 11]. This leads to:

$$\psi = \frac{m\tilde{\beta}}{XZ_0} \cdot \frac{J_m(X)}{J'_m(X)}
 \tag{3}$$

with m as the azimuthal mode index, $\tilde{\beta}$ as the normalized phase constant with $\tilde{\beta} = \beta/k$, $k = 2\pi/\lambda$ as the wavenumber and $Z_0 = 120\pi \Omega$ as the free space wave impedance. Ohmic losses are neglected here.

In the following, the eigenmodes are always normalized to $P_z = 1$ W, with P_z as the mode power in the direction of propagation. For this purpose, the pointing vector [28] is integrated over the waveguide cross-section:

$$P_z = \frac{1}{2} \cdot \int_A (\vec{E} \times \vec{H}^*) \times \vec{z} \, d\vec{A}
 \tag{4}$$

with $\vec{z} = (0, 0, 1)^T$ as the normal vector in the direction of propagation. Then, the field components in Eq. (1) are normalized in respect to $\sqrt{P_z}$.

The eigenvalues within a corrugated circular waveguide can be calculated as discussed in detail in [10, 11, 29, 30]. For the HE₁₁ hybrid mode, fulfilling the balanced hybrid mode condition, follows: $X = 2.404826$.

2.3 Mode decomposition

An arbitrary electromagnetic field shall be represented as:

$$\vec{E} = \sum_{\infty} (\vartheta_n^+ + \vartheta_n^-) \cdot \vec{e}_n \vec{H} = \sum_{\infty} (\vartheta_n^+ - \vartheta_n^-) \cdot \vec{h}_n
 \tag{5}$$

with $\vartheta_n^{+/-}$ as the n th complex mode amplitude in forward/backward direction and \vec{e}_n/\vec{h}_n as the electromagnetic field components of the n th corresponding eigenmode. As introduced in section 2.2, all eigenmodes are normalized to $P_z = 1$ W, here. With fundamental manipulations and the power orthogonality condition, $\int_A (\vec{e}_{\perp n} \cdot \vec{e}_{\perp m}^*) \, d\vec{A} = 0$ for $n \neq m$ [31, 32], follows:

$$\vartheta_m^+ = \frac{1}{4} \cdot \left(\frac{1}{Z_m} \cdot \int_A (\vec{E}_{\perp} \cdot \vec{e}_{\perp m}^*) \, d\vec{A} + Z_m \cdot \int_A (\vec{H}_{\perp} \cdot \vec{h}_{\perp m}^*) \, d\vec{A} \right)
 \tag{6}$$

$$\vartheta_m^- = \frac{1}{4} \cdot \left(\frac{1}{Z_m} \cdot \int_A \left(\vec{E}_\perp \cdot \vec{e}_{\perp m}^* \right) d\vec{A} - Z_m \cdot \int_A \left(\vec{H}_\perp \cdot \vec{h}_{\perp m}^* \right) d\vec{A} \right) \quad (7)$$

with:

$$Z_m = \frac{1}{2} \cdot \int_A \left| \vec{e}_{\perp m} \right|^2 d\vec{A} = \left(\frac{1}{2} \cdot \int_A \left| \vec{h}_{\perp m} \right|^2 d\vec{A} \right)^{-1} \quad (8)$$

as the normalized mode impedance of the corresponding eigenmodes. The integrals are executed in respect of the waveguide cross-section (for $r \leq a$).

Based on Eqs. (6) and (7), an arbitrary electromagnetic field can be decomposed in corresponding forward/backward travelling eigenmodes. Just the transversal field components are required, thereby.

3 Design procedure

In this section the design procedure for the broadband high-power TE₁₁ ↔ HE₁₁ mode converter is addressed. The Subsection 3.1 introduces the principle design approach. Corresponding simulation results are addressed in the Subsection 3.2.

3.1 Principle approach

Figure 2 shows the principle flow diagram of the proposed design procedure. The kernel is a genetic algorithm [33] used to solve a global optimization problem. The optimization problem is defined due to a cost-function with the scalar output parameter C . The principle concept of a genetic algorithm is inspired by a natural selection process [33–35]: Based on an initial population of individuals, an evolution is set in motion. This is an iterative process, where each iteration leads to a new generation. Within each iteration the cost function for each individual is carried out and evaluated. Due to a stochastic process, the most suitable individuals are selected and used as the starting point for the upcoming generation. For the next generation, the selected individuals are reproduced and mutated (e.g. randomly). Then, again, for each individual, the cost function is carried out, and the most suitable individuals are selected stochastically for the next generation. The optimization terminates, if convergence is detected. Besides a proper initial population, the genetic algorithm is initialized with proper boundary conditions. Here, these are the waveguide diameters at the input/output and a permitted range of the mode converter length L . A more detailed consideration of the genetic algorithm is out of scope of the present paper. A comprehensive consideration is found in [33–35]. Here, the MATLAB implementation discussed in detail in [36] is used.

The parameters, optimized due to a genetic algorithms, are named chromosomes [33]. Here, the chromosomes represent the geometry of the considered mode converter. However, to reduce the required amount of calculation, the chromosomes are limited to a few net points, here. The complete geometry is calculated based on an interpolation within the cost-function.

The cost-function parameter C is calculated as:

$$2C = 1 - \left(\left(|\vartheta^+|^2 \right)_{z=L} - \left(\sum_m |\Gamma_m|^2 \right)_{z=0} \right) \quad (9)$$

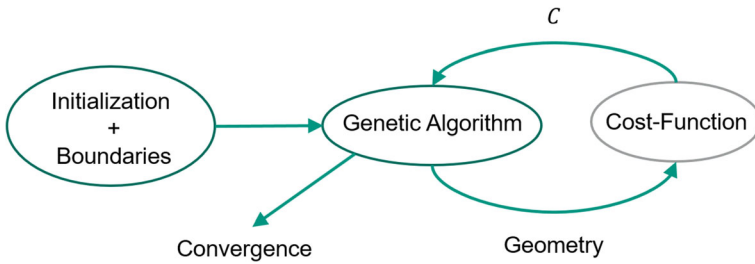


Fig. 2 Principle flow diagram of the design procedure.

with ϑ^+ as the complex HE_{11} mode amplitude in forward direction at the mode converter output ($z = L$) and Γ_m as the complex reflection coefficient of the m th TE/TM eigenmode at the input of the mode converter ($z = 0$).

Within the optimization, Eq. (9) is carried out at a single frequency. In principle, also a multifrequency cost-function could be considered. However, the design procedure based on Eq. (9) showed inherent broadband frequency behaviour for corresponding mode converters. Therefore, to reduce the required amount of calculation, a multifrequency cost function was waived. Equation (9) is carried out at the centre frequency of 96 GHz.

Figure 3 shows the principle calculation flow of the cost-function parameter C . The flow chart represents the grey circle in Fig. 2.

The input parameters are the chromosomes, used for optimization. As mentioned, those represent single net points of the mode converter geometry. The complete geometry is calculated based on an interpolation, which is carried out in the first step in Fig. 3. Based on the mode converter geometry, the corresponding scattering matrix [28] of the structure is calculated. The scattering matrix links the incoming and outgoing electromagnetic waves of the structure. To consider multimode devices, the scattering matrix can be extended to the generalized scattering matrix [37–39]. For corresponding calculations, a KIT implementation [39] of the scattering matrix formalism, based on [37, 38], was extended and modified for the present application. As output, the reflection and transmission coefficients of the considered eigenmodes as well as their coupling within the structure are calculated. A more detailed consideration of such a scattering matrix formalism is out of scope of the present paper. A comprehensive consideration is found in [37–39]. The utilized scattering matrix code was verified in [39] with multiple simulation structures and different full wave simulation tools (e.g. CST Microwave Studio [40]).

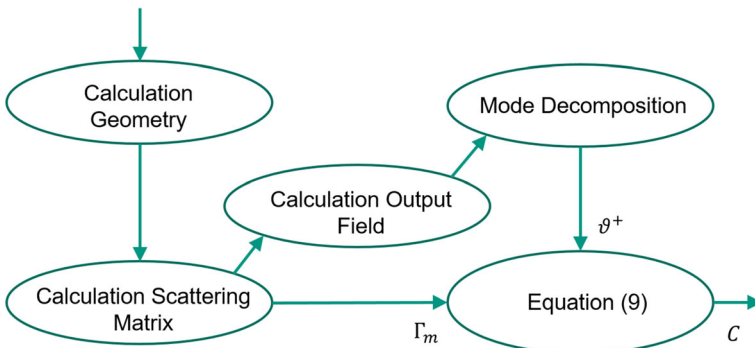


Fig. 3 Principle flow chart of the cost function calculations

To calculate the cost-function parameter C , the single reflection coefficients at the mode converter input as well as the HE_{11} mode content at the mode converter output are required. The reflection coefficients are directly provided by the scattering matrix formalism [37, 39]. All of the considered reflection coefficients at the input ($z=0$) are summed up to get the overall power reflection at the mode converter input. In ideal applies: $\sum |\Gamma_m|^2 = 0$ at $z=0$, which implies no reflected power at the mode converter input.

To calculate the HE_{11} mode content, first the electromagnetic field components at the mode converter output are calculated as superposition of the calculated TE/TM mode content, provided by the scattering matrix formalism [37, 39]. Using the equations from subsection 2.3 and the derived HE_{11} eigenmodes from subsection 2.2, the required HE_{11} mode content can be calculated. In ideal applies: $|\vartheta_+|^2 = 1$ at $z=L$, which implies a pure HE_{11} mode at the mode converter output.

Based on the calculations on the reflection coefficients and the HE_{11} mode content, Eq. (9) can be carried out and used for optimization. In ideal applies: $C=0$, which implies that the whole TE_{11} mode power at the mode converter input is coupled into the HE_{11} mode at the mode converter output.

3.2 Results

Figure 4 shows the geometry of the optimized $TE_{11} \rightarrow HE_{11}$ mode converter. The red circles represent the chromosomes, used for optimization. Note that the geometry is not described due to an analytical function but corresponds to numerical optimized data points.

The specified input diameter is $D = 2.749$ mm which corresponds to a standard waveguide flange [41] which fits to an optimized helical interaction waveguide. The specified output diameter is $D = 31.75$ mm which corresponds to a standard corrugated waveguide diameter

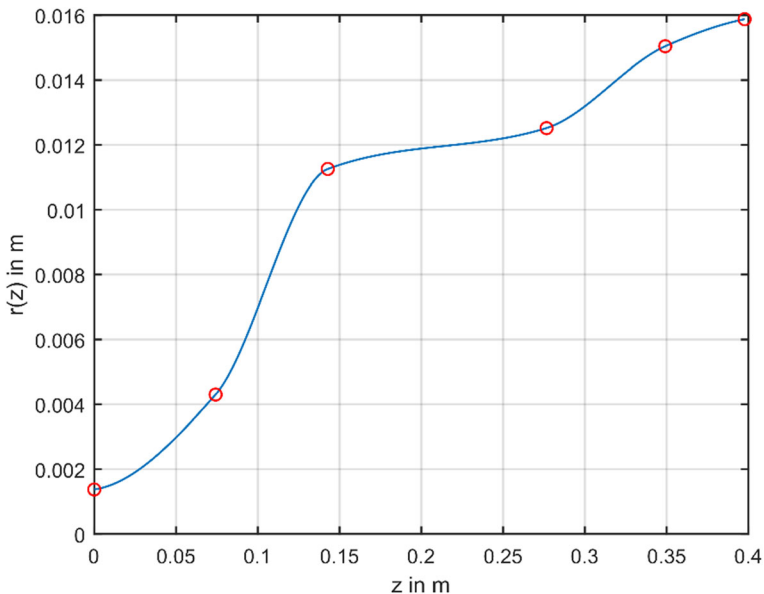


Fig. 4 Radius profile along the optimized $TE_{11} \rightarrow HE_{11}$ mode converter. The red circles represent the single chromosomes, used for optimization

[42]. The position and the value of the first net point were fixed ($D_1 = 2.749$ mm, $z_1 = 0$) as well as the value of the last net point ($D_6 = 31.75$ mm). Therefore, five net point positions and four net point values had to be optimized. The mode converter length was optimized to $L = 39.81$ cm with $z_6 = L$. Within the cost function, the geometry is considered with 1000 steps, which ensures convergence in respect of a smooth waveguide profile [39].

Figure 5 shows the corresponding simulations results in respect of the HE_{11} mode content at the mode converter output, within the frequency range from 90 GHz to 100 GHz. The squared absolute value ($|\vartheta^+|^2$, colored in brown) as well as the phase history ($\text{angle}(\vartheta^+)$, colored in blue) is shown. Due to the applied normalization, the squared absolute value of the complex mode amplitude corresponds directly to the relative mode content.

The calculated mode content shows the broadband frequency behaviour of the design. Within the frequency range from 92 GHz to 100 GHz, the HE_{11} mode content is always higher than 98.6 %. Inside this frequency band, the mode content is even better and reaches ≈ 99.7 % at ≈ 95 GHz.

For broadband frequency operation, a high mode content as well as a linear phase response is essential. A non-linear phase response would lead to a varying group velocity [28] which may cause critical distortions. In respect of a broadband radar sensor, this may impair the geometrical radar resolution [43, 44]. However, Fig. 5 shows a close to ideal linear phase response of the designed mode converter and therefore, again, broadband frequency behaviour. No critical distortion for broadband frequency operation has to be expected.

For the shown mode converter geometry, the optimization procedure leads to a cost-function parameter $C = 4.2041e-3$. The overall reflection coefficient at the mode converter input, calculated in respect of all considered eigenmodes, is far below -30 dB and can be neglected. In total, 122 TE/TM modes were considered within the scattering matrix formalism. Due to the symmetry within the circular structure and the TE_{11} input mode, the calculations could be limited to the TE_{1n}/TM_{1n} modes [37–39] with $n = 1 \dots 61$.

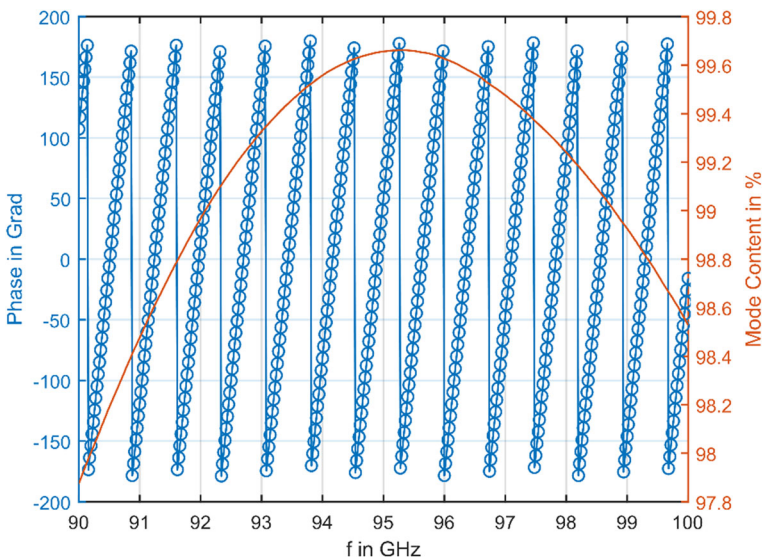


Fig. 5 Complex HE_{11} mode amplitude at the mode converter output. Phase response (blue circles). Squared absolute value (brown curve)

Note that the present paper focused on the elaborated design procedure for broadband high-power $TE_{11} \leftrightarrow HE_{11}$ mode converters. The presented mode converter design will be experimentally proven and discussed in more details later, when the mode converter is manufactured as well as the corresponding test setup is built up. Due to the direct coupling into a corrugated waveguide, simple far-field radiation pattern measurements will not lead to adequate results. An advanced test setup has to be build up, which will be addressed in an upcoming paper as well as corresponding measurements components like advanced broadband mode coupler for precise mode content determination within a corrugated waveguide.

4 Conclusion

The present paper addresses the design procedure for a broadband high-power $TE_{11} \leftrightarrow HE_{11}$ mode converter. The mode converter is realized within a smooth circular waveguide which simplifies the manufacturing and allows the integration of an electron collector within the mode converter. The mode converter is designed for a W-band (92 GHz to 100 GHz) helical gyro-TWT which is intended to be used for an advanced broadband high-power radar sensor for space debris observation in the low earth orbit (LEO). The design procedure is based on numerical optimization using a genetic algorithm and the scattering matrix formalism.

Within the considered frequency band, a high HE_{11} mode content as well as a linear phase response could be achieved. This is essential for broadband frequency operation.

Future research activities will address the manufacturing of the mode converter as well as the design and the construction of a prober test system at KIT for such mode converters. Furthermore, more detailed simulation in respect of the integration of an electron collector will be carried out.

Funding Open Access funding enabled and organized by Projekt DEAL.

Open Access This article is licensed under a Creative Commons Attribution 4.0 International License, which permits use, sharing, adaptation, distribution and reproduction in any medium or format, as long as you give appropriate credit to the original author(s) and the source, provide a link to the Creative Commons licence, and indicate if changes were made. The images or other third party material in this article are included in the article's Creative Commons licence, unless indicated otherwise in a credit line to the material. If material is not included in the article's Creative Commons licence and your intended use is not permitted by statutory regulation or exceeds the permitted use, you will need to obtain permission directly from the copyright holder. To view a copy of this licence, visit <http://creativecommons.org/licenses/by/4.0/>.

References

1. S. Samsonov, et al., "CW Operation of a W-Band High-Gain Helical-Waveguide Gyrotron Traveling-Wave Tube", *IEEE Electronic Device Letters*, Vol. 41, No. 5, 773-776 (2020)
2. G. Denisov, et al., "Gyro-TWTs with Helically Corrugated Waveguides: Overview of the Main Principles", *International Conference on Infrared, Millimeter and Terahertz Waves*, Paris, France, 1-3 (2019)
3. M. Czerwinski and J. Usoff, "Development of the Haystack Ultrawideband Satellite Imaging Radar", *Lincoln Laboratory Journal*, Vol. 21, No. 1, 28-44, (2014).
4. M. MacDonald et al., "The HUSIR W-Band Transmitter", *Lincoln Laboratory Journal*, Vol. 21, No. 1, 106-114 (2014).
5. J. Eshbaugh et al., "HUSIR Signal Processing", *Lincoln Laboratory Journal*, Vol. 21, No. 1, 115-134 (2014).

6. S. Samsonov et al., "Cascade of Two W-Band Helical-Waveguide Gyro-TWTs with High Gain and Output Power: Concept and Modeling", *IEEE Transaction on Electron Devices*, Vol. 64, No. 3, 1305-1309 (2017).
7. J. Doane, "Propagation and Mode Coupling in Corrugated and Smooth-Wall Circular Waveguides", *Infrared and Millimeter Waves*, Vol. 13, Ch. 5, 123-170 (1985).
8. J. Doane, "Design of Circular Corrugated Waveguides to Transmit Millimeter Waves at ITER", *Fusion Science and Technology*, Vol. 53, No. 1, 159-173 (2008).
9. J. Anderson et al., "Beyond Fusion: The Application of Fusion-Based Microwave Technology to Other Industries", *International Conference on Infrared, Millimeter and Terahertz Waves*, Paris, France, 1-2 (2019).
10. P. Clarricoats and A. Olver, *Corrugated Horns for Microwave Antennas*. IEE Electromagnetic Waves Series 18 (1984)
11. P. Clarricoats et al., "Propagation and Radiation Behavior of Corrugated Feeds: Part 2, Corrugated Conical-Horn Feed", *Proceedings of the Institution of Electrical Engineers*, Vol. 118, No. 9, 1177-1186 (1971).
12. J. Doane, "Transitions to Oversized Corrugated Waveguides", *International Conference on Infrared and Millimeter Waves*, Monterey, USA (1999).
13. <http://www.ga.com/transitions-for-testing-high-power-waveguide> (11. May 2020)
14. J. Doane and C. Moeller, "HE11 Mitre Bends and Gaps in a Circular Corrugated Waveguide", *International Journal of Electronics*, Vol. 77, No. 4, 489-509 (1994).
15. E. Kowalski, "Miter Bend Loss and High Order Mode Content Measurements in Overmoded Millimeter-Wave Transmission Lines" Master-Thesis, Massachusetts Institutes of Technology (2010).
16. S. Mishakin, et al., "A Helical-Waveguide Gyro-TWT at the Third Cyclotron Harmonic", *IEEE Transaction on Electron Devices*, Vol. 62, Nr. 10, 3387-3392 (2015).
17. M. Thumm et al., "Computer-Aided Analysis and Design of Corrugated TE11 to HE11 Mode Converters in Highly Overmoded Waveguides", *International Journal of Infrared and Millimeter Waves*, Vol. 6, No. 7, 577-597 (1985).
18. M. Thumm et al., "Design of Short High-Power TE11-HE11 Mode Converters in Highly Overmoded Corrugated Waveguides", *Transaction on Microwave Theory and Techniques*, Vol. 39, No. 2, 577-597 (1991).
19. L. Zhang, et al. "Optimization and Measurement of a Smoothly Profiled Horn for a W-Band Gyro-TWA", *IEEE Trans. Electron Devices*, Vol. 64, No. 6, 2665-2669 (2017).
20. W. He, et al., "The Development of Broadband Millimeter-Wave and Terahertz gyro-TWA" *Terahertz Science & Technology*, Vol. 13, No. 3, 90-110 (2020).
21. G. Denisov, et al., "Gyro-TWT with a Helical Operating Waveguide: New Possibilities to Enhance Efficiency and Frequency Bandwidth", *IEEE Transaction on Plasma Science*, Vol. 26, No. 3, 508-518 (1998).
22. V. Bratman, et al., "High-Efficiency Wideband Gyro-TWTs and Gyro-BWOs with Helically Corrugated Waveguides", *Radiophysics and Quantum Electronics*, Vol. 50, No. 2, 95-107 (2007).
23. S. Cooke and G. Denisov, "Linear Theory of a Wide-Band Gyro-TWT Amplifier Using Spiral Waveguide", *IEEE Transaction on Plasma Science*, Vol. 26, No. 3, 519-530 (1998).
24. K. Chu, "The Electron Cyclotron Maser", *Reviews of Modern Physics*, Vol. 76 (2004).
25. P. Sprangle and A. Drobot, "The Linear and Self-Consistent Nonlinear Theory of the Electron Cyclotron Maser Instability", *IEEE Transaction on Microwave Theory and Techniques*, Vol. 25, No. 6, 528-544 (1977).
26. G. Denisov, et al., "Gyrotron Traveling Wave Amplifier with a Helical Interaction Waveguide", *Physical Reviews Letters*, Vol. 81, No. 25 (1998).
27. S. Samsonov, et al., "CW Ka-Band Kilowatt-Level Helical-Waveguide Gyro-TWT" *IEEE Transaction on Electron Devices*, 2250-2255 (2012).
28. D. Pozar, *Microwave Engineering: Fourth Edition*, John Wiley & Sons, 2010.
29. D. Haas et al., "Calculations on Mode Eigenvalues in a Corrugated Waveguide with varying Diameter and Corrugation Profile", *Journal of Infrared, Millimeter and Terahertz Waves*, submitted (2020).
30. P. Clarricoats et al., "Propagation and Radiation Behavior of Corrugated Feeds: Part 1, Corrugated Waveguide Feed", *Proceedings of the Institution of Electrical Engineers*, Vol. 118, No. 9, 1177-1186 (1971).
31. J. Jackson, *Classical Electrodynamics*. John Wiley & Sons, 1975.
32. S. Mahmoud, *Electromagnetic Waveguides: Theory and Applications*. IET Electromagnetic Waves Series 32, 2006.
33. O. Kramer, *Genetic Algorithm Essentials*, Springer, 2017.
34. Y. Rahmat-Sami and E. Michielssen, *Electromagnetic Optimization by Genetic Algorithms*, Wiley Interscience, 1999.

35. B. Plaum, et al., Optimization of Oversized Waveguide Components Using a Genetic Algorithm, *Fusion Engineering and Design*, Vol. 53, 499-503 (2001).
36. <https://de.mathworks.com/help/gads/ga.html> General Scattering Matrix Code (15. November 2020)
37. J. Neilson, et al., Determination of the resonant frequencies in a complex cavity using the scattering matrix formulation. *IEEE Transactions on Microwave Theory and Techniques*, Vol. 37, No. 8, 1165–1170 (1989)
38. J. Pace, “The Generalized Scattering Matrix Analysis of Waveguide Discontinuity Problems” Rep. 1, Antenna Laboratory, University of Illinois, USA, 1964.
39. M. Engler, “Development of a Flexible Scattering Matrix Code for the Design and Optimization of Circular Waveguide Components”, Master Thesis, Karlsruhe Institute of Technology (KIT), Germany, 2018.
40. CST Microwave Studio 2008: Workflow & Solver Overview.
41. <https://www.eravant.com/wr-10-rectangular-to-0-110-diameter-circular-waveguide-mode-transition> (15. November 2020).
42. <http://www.ga.com/straight-corrugated-waveguides> (11. Mai 2020)
43. F. Perez-Martinez, et al., “Group Delay Effects on the Performance of Wideband CW-LFM Radars”, *IEE Proceedings-Radar, Sonar and Navigation*, 95-100 (2001).
44. C. Esposito, et al., “Geometric Distortions in FMCW SAR Images due to Inaccurate Knowledge of Electronic Radar Parameters: Analysis and Correction by Means of Corner Reflectors”, *Remote Sensing of Environment* (2019).

Publisher’s Note Springer Nature remains neutral with regard to jurisdictional claims in published maps and institutional affiliations.